2T3C HCA, a new hollow cylinder device using Digital Image Correlation to measure properties of interfaces between asphalt layers

T. Attia, H. Di Benedetto, C. Sauzéat, S. Pouget

2T3C HCA, a new hollow cylinder device using Digital Image Correlation to measure properties of interfaces between asphalt layers

T. Attia[1*], H. Di Benedetto[1], C. Sauzéat[1] and S. Pouget[2]

[1] University of Lyon / Ecole Nationale des Travaux Publics de l'Etat (ENTPE), LTDS (CNRS 5513), France
[2] Eiffage Infrastructures, Research & Innovation Department, France
*thomas.attia@entpe.fr

Abstract. To improve pavement resistance, asphalt concrete layers are bonded together with a tack coat. A new device has been developed to describe the mechanical behavior of interfaces between asphalt concrete layers. The 2T3C Hollow Cylinder Apparatus (2T3C HCA) can apply torsion and tension-compression to hollow cylinder samples composed of two asphalt concrete layers with a tack coat in between. Normal and shear stresses can be applied independently with any type of loading (monotonic or cyclic). In addition to global measurements, a local optical method, based on Digital Image Correlation (DIC), is used to observe the deformation of the interface. The first interface characterization results are presented in this paper.

Keywords: Pavement layers, Asphalt concrete, Interface behavior, Hollow Cylinder Apparatus (HCA), Digital Image Correlation (DIC), Experimental results

Declarations of interest: none

1 Introduction

Pavement sustainability is a major issue both economically and environmentally. Building long-life pavements that require little maintenance saves money and energy. Pavement structure is constituted by multiple layers made in different materials such as cement concrete or asphalt concrete. Each layer has a different function in the structure. The top layer, the wearing course, guarantees the adherence with the tires. The layer under the wearing course, the base course, diffuses in the lower layers the loads caused by traffic and climate. In pavements subjected to high traffic, both of these layers are generally made in asphalt concretes. Numerical simulations [1,2] showed that binding the layers between them reduces the maximal deformation in the pavement improving its lifetime. In order to achieve this bonding, a tack coat, often made of bitumen emulsion, is applied at the interface between the two layers. Assuming the tack coat has been correctly applied, the asphalt concrete layers are considered perfectly bonded in some of the current pavement design methods [3,4]. However, premature degradations linked with the debonding of the layers have been reported [5,6]. In this case, the pavement is subjected to loads it is not designed to resist to, implying a shortened lifetime. It is also possible that even for tack coat applied carefully and with a good dosage the interface will fail in fatigue before the asphalt concretes [7]. Yet, interface fatigue behavior is not considered in the design methods. The study of the mechanical behavior of interfaces between asphalt concrete layers is then critical to help designing better roads.

The mechanical testing of interfaces began in the 1970's [1,8] and has gained more and more importance with time. Traffic and climate loads create complex stress states in the pavement. Different types of tests were developed to evaluate the bond strength at the interface between two asphalt pavement layers: tensile tests [9], shear tests [8,10-12], wedge splitting tests [9,13], torque test [14] (for broader overviews, see [15,16]). The shear tests are the most common and some of them can also apply compressive or tensile stress. Most of these tests aimed at evaluating only the shear strength of interfaces, which is the highest possible shear stress the interface can endure before failing. The influence of factors such as temperature [17], normal stress application [10], nature and dosage of tack coat [18] have been investigated. Several shear tests are used to assess interface fatigue properties under cyclic shear loadings [2, 19-22] in order to obtain the fatigue law of interfaces for different test conditions or different materials. All these shear tests are inhomogeneous: the shear stress is not uniform at the interface.

It appears that a powerful test on interfaces should, (i) be able to apply shear and compressive/tensile stress, in monotonic or cyclic modes, to reproduce the actual pavement conditions, and (ii) be homogeneous in order to be analyzed correctly.

This paper presents the development of a new device to test interfaces between pavement layers. It is called 2T3C Hollow Cylinder Apparatus (2T3C HCA) and can apply torsion and tension-compression to hollow cylinder samples composed of two asphalt concrete layers. This apparatus uses 3D Digital Image Correlation (3D DIC) to observe the behavior of the interface. Additionally, the first experimental characterization of the viscoelastic behavior of asphalt concretes and of the interface using 2T3C HCA is presented.

This work is part of the industrial chair Eiffage/ENTPE dedicated to pavement materials and structures.

2 Description of 2T3C Hollow Cylinder Apparatus (2T3C HCA)

2.1 Hollow cylinder sample

Applying a torque to a cylinder creates an inhomogeneous shear stress field. For example, if the material is elastic linear isotropic, the shear stress varies linearly with the radius, being nil at the center of the cylinder. In a hollow cylinder, the inner part of the cylinder is removed. If the thickness left is thin enough then one can consider that the shear stress is homogeneous with a good approximation [23] which ensures simplified but accurate test analysis. This is why a hollow cylinder apparatus is relevant to study interfaces behavior. Hollow cylinder tests have been broadly used for the testing of soils and granular materials [24,25] and they have also been used for the study of asphalt concrete [26-28]. However, no example of application to the study of interfaces between asphalt layers was found in the literature.

A new hollow cylinder apparatus has been developed at the University of Lyon/ENTPE: it is called 2T3C (in French, *Torsion-Traction-Compression sur Cylindre Creux*) Hollow Cylinder Apparatus (2T3C HCA). It allows applying torsion and tension-compression to hollow cylinder samples. The sample dimensions are: height of 125 mm, internal diameter of 122 mm, external diameter of 172 mm and thickness of 25 mm. The sample section area is 115.5 cm^2. The samples are composed of two asphalt concrete layers with a tack coat at the interface located in the middle of the sample (Figure 1). The external diameter and the height are chosen considering fabrication constraints. The selected thickness is a compromise between having a thickness large enough compared to the maximum aggregate size and small enough to obtain the maximum shear stress applicable and a good shear stress homogeneity. The ratio between internal radius and external radius is 0.71, this value is between 0.65 and 0.82, the range recommended for a reasonable assumption of homogeneity of shear stress for a hollow cylinder test [23].

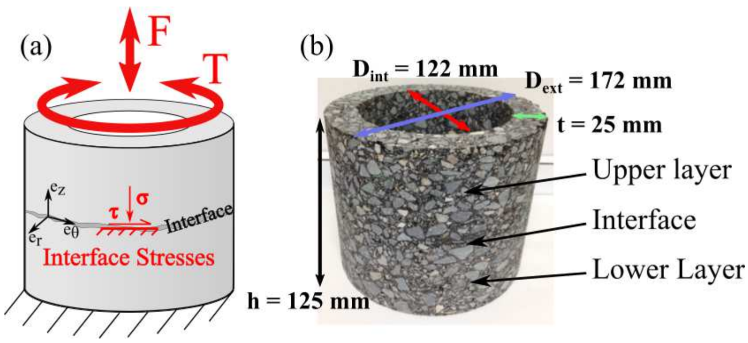

Fig. 1. 2T3C HCA hollow cylinder samples: (a) schematic, (b) picture

2.2 Sample preparation

In this section, the fabrication of laboratory samples is presented (Figure 2) but samples from real pavements cored *in situ* can also be tested with the 2T3C HCA. A slab with two layers and a tack coat at the interface is created using the French wheel compactor [29] (Figure 3). This is done in three steps. First, half a slab (600x400x75 mm^3) of the material representing the base course, the lower layer, is compacted. Then, after a 24 h rest period, a tack coat made of asphalt emulsion is applied on the surface of the lower layer using a brush (Figure 3). Finally, after another 24 h rest, the upper layer is compacted using the compacting wheels again to get the complete slab (600x400x150 mm^3).

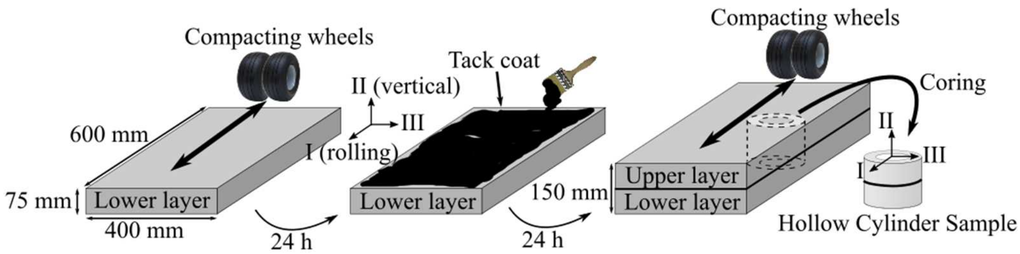

Fig. 2. Process to obtain hollow cylinder sample from a two layered slab with a tack coat at the interface

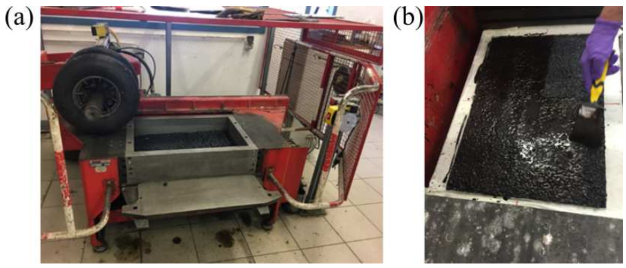

Fig. 3. French wheel compactor [29] (a) and tack coat application with brush (b) for the sample preparation

First the inside of a hollow cylinder is cored and then the outside. The two ends of the sample are then sawed to guarantee their planarity. A speckle pattern consisting of sprayed black paint over a thin white paint coat is applied on the surface of the sample for Digital Image Correlation (DIC) analysis. Samples are glued to aluminum plates using epoxy resin. A specially designed gluing device ensures that the axis of the hollow cylinder is coincident with the axes of the plates and thus of the hydraulic press.

2.3 2T3C HCA measuring systems

Torsion and tension-compression are applied to the samples using a servohydraulic press. Load cells measure the axial force up to ± 100 kN (with an accuracy of 0.010 kN) and the torque up to ± 2 kNm (accuracy of 0.1 Nm). Axial loadings and rotation loadings can be applied independently with any type of loading history: monotonic or cyclic (up to 10 Hz), stress or displacement controlled, following any load path. The sample with the plates, fixed to the press, is located in a thermal chamber with a temperature range from – 20 °C to + 60 °C (Figure 4). The temperature is measured on the surface of the sample with two PT100 sensors, one on the inside surface of the sample and one on the outside surface of the sample (Figure 5) in order to verify the homogeneity of the temperature field in the sample.

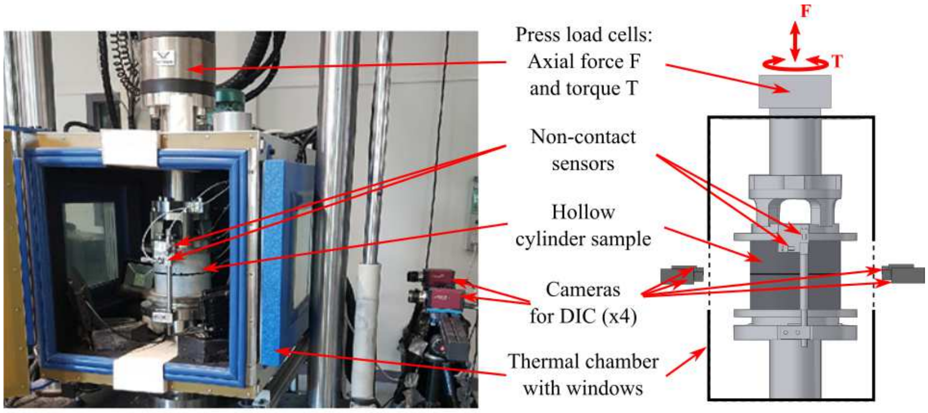

Fig. 4. Picture and scheme of the 2T3C HCA with measuring systems

Two pairs of non-contact sensors measure the global displacements (in rotation and axial direction) between the top and the bottom of the samples. They can measure displacements with an accuracy of about 0.1 µm on a 1000 µm range. Sensors are fixed to the top plate and their aluminum target is fixed to the bottom plate. On each side of the sample there is one pair of non-contact sensors with one sensor that measures vertical displacement and one sensor that measures the displacement related to the rotation (Figure 5). The value of global vertical displacement is taken as the average of the values of the two sensors measuring the vertical displacement (V1 and V2 in Figure 5). The global horizontal displacement related to the rotation is obtained in a similar way. Tests can be performed under displacement control using the non-contact sensors values.

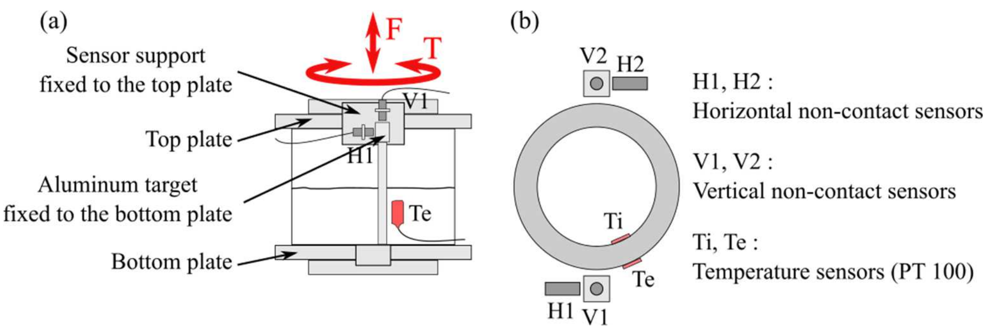

Fig. 5. 2T3C HCA sample instrumentation: (a) Side view, (b) Top view

In addition to global measurements, a local optical measurement method, the 3D DIC is used in the 2T3C HCA. This method finds the displacement field in the three dimensions on the surface of the sample and is presented in the next section.

2.4 Analysis from Digital Image Correlation

Two pairs of CCD cameras take digital pictures of 4 Mpx of each side of the sample (Figure 4) with a maximum acquisition frequency of 10 Hz. In each pair, the optical axii of the two cameras form an angle of 30° in order to use 3D DIC. Cameras are located outside the thermal chamber, 600 mm from the surface of the sample. At this distance and considering the CCD sensor characteristics, one pixel of a picture represents 150 µm of material. The thermal chamber has windows on its sides, which makes it possible to take pictures of the sample during tests at controlled temperature.

DIC principle is schematized in Figure 6. During a test, grayscale pictures of the sample are taken at different levels of deformation. The first image, representing the reference state, is called the reference picture. The goal of DIC is to obtain the displacement of the points at the surface of the sample at each level of deformation, *i.e.* for each picture, relatively to the reference state. For each pixel of the reference picture located in the area of interest (area where displacements are researched), a subset of the picture is selected. It is a square, usually a dozen pixels long, centered around the pixel. A correlation algorithm finds the subset of the deformed pictured that looks the most like the subset in the reference picture and deduces the displacement of the pixel [30].

There needs to be a very contrasted and random pattern at the surface of the studied material. Asphalt concretes samples are naturally not well-contrasted. A speckle pattern, as the one described in section 2.2, is usually applied on the samples surface [31]. DIC has been used for the study of asphalt concretes cracking behavior [32] and rarely for the study of interfaces [33]. It has proved to be a consistent tool in the study of deformations of many materials such as cement concrete [34,35], glass [36] or metals [37].

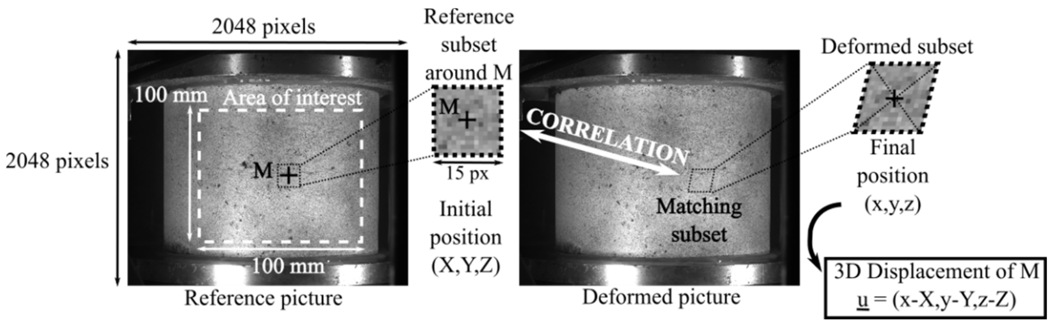

Fig. 6. 3D Digital Image Correlation: determination of 3D displacements of each point M of the area of interest

For 3D DIC, two pictures of the same surface taken from different angles are needed at each state of deformation. An algorithm between the two pictures associates a spatial position to any pixel of the images. Displacements in the three dimensions are found using the correlation algorithm between reference and deformed states on one image of each pair [38].

The Vic-3D® software developed by Correlated Solutions is used for 3D DIC measurements in the 2T3C HCA. It computes displacements in the three dimensions on the hollow cylinder surface and expresses them in the cylindrical coordinate system related to the hollow cylinder (u_r, u_θ, u_z, Z being the axis of the cylinder). The heterogeneity of the asphalt concretes induces high spatial variability of displacements due to the difference in mechanical behaviors of bitumen and aggregates. A specific analysis developed at the ENTPE computes the three strain tensor components ($\varepsilon_{\theta\theta}$, ε_{zz}, $\varepsilon_{\theta z}$) of both asphalt concrete layers and the displacement gaps at the interface (Δu_z, Δu_θ) throughout a test, anytime a picture is taken. Strain is obtained with an accuracy of about 1 µm/m and displacement gaps with an accuracy of 0.1 µm.

For ε_{zz} computation, horizontal strips (100 mm long and 3 mm thick) are drawn on the pictures as illustrated in Figure 7. The number of strips in each layer depends on the sample dimensions (between 10 and 15). For each state of deformation, the displacement component u_z is averaged on each strip and the average value is affected to the coordinate Z of the center of the strip. The slopes of the lines obtained with linear regressions in the diagram Z-u_z, one in each layer, give the strain components ε_{zz} in both asphalt concretes. These two lines do not intersect at the interface and the gap between them at the level of the interface (located visually) defines the axial displacement gap Δu_z.

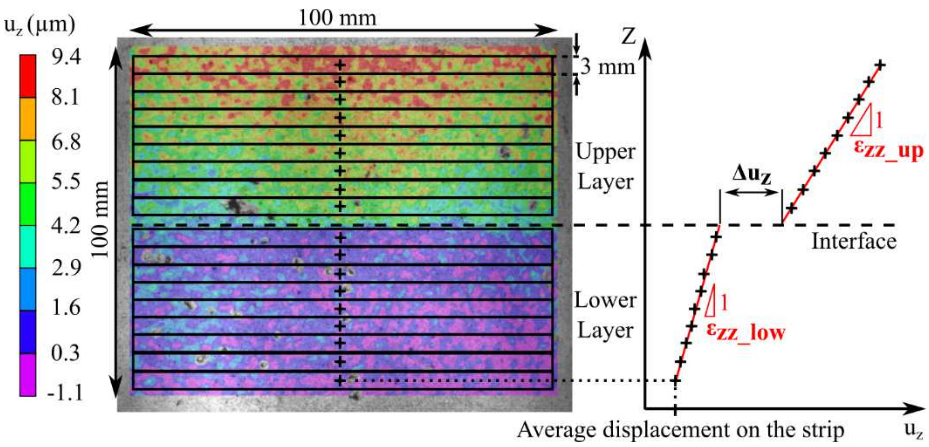

Fig. 7. Vertical displacement u_z measurements from DIC and illustration of computation of ε_{zz} in both asphalt layers and of the displacement gap Δu_z at the interface (picture at 12.5 µm in extension)

The strain tensor component $\varepsilon_{\theta z}$ is obtained using the same method as above, but replacing the displacement component u_z with u_θ. The displacement gap Δu_θ is then found. In the analysis method presented in this paper, the interface thickness is considered nil, corresponding to a structural point of view. However, it is also possible to use DIC to look at the interface from a closer range and to define the thickness of the interfacial transition zone [33]. The latter approach can be used to model interfaces at a smaller scale, taking precisely into account aggregate interlocking.

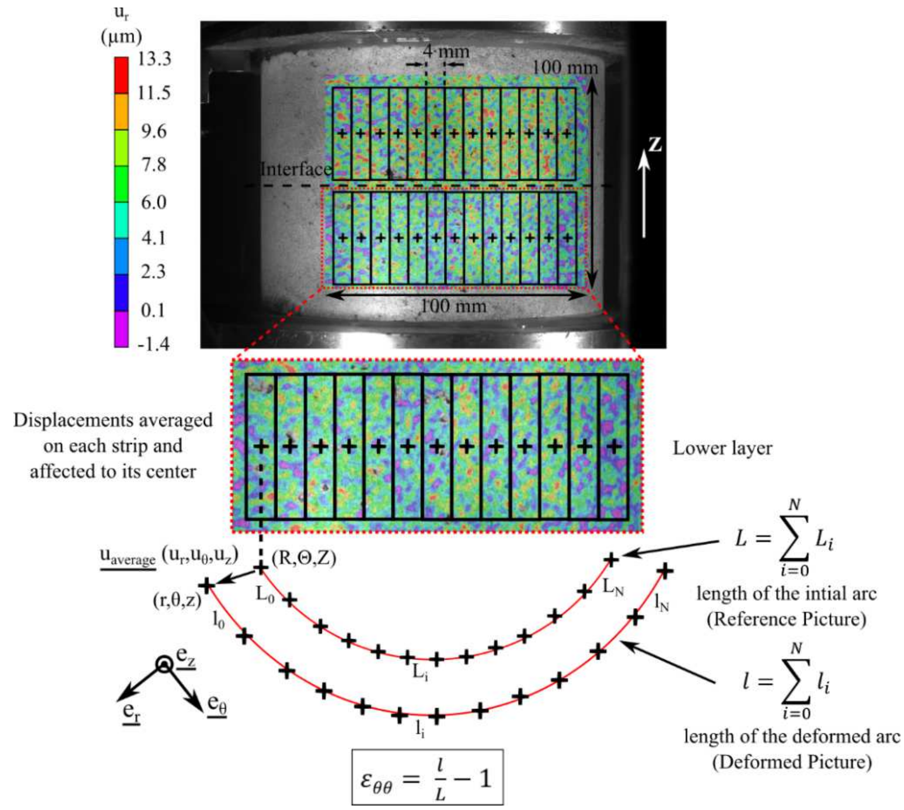

Fig. 8. Computation of $\varepsilon_{\theta\theta}$ in one asphalt layer (picture at 12.5 µm in compression)

Assuming that the hollow cylinder remains a hollow cylinder during a test, the strain tensor component $\varepsilon_{\theta\theta}$ is equal to the relative variation of external perimeter of the cylinder. The computation of $\varepsilon_{\theta\theta}$ is illustrated in Figure 8. In each layer, about 20 vertical strips (4 mm thick and 45 mm high) are drawn on the pictures so that the central points of the strips are situated along an arc. Its length in the reference picture can be calculated. For each level of deformation, *i.e.* for each picture, the three displacement components (u_r, u_θ, u_z) of the points in each strip are averaged and affected to the center of the strip. The coordinates of the center after transformation are obtained using this averaged displacement. The centers of the strips after transformation are situated along a deformed arc, the length of which is also calculated. The strain tensor component $\varepsilon_{\theta\theta}$, equal to the relative variation of arc length, is thus obtained at each state of deformation in both asphalt concretes.

In the 2T3C HCA, two pairs of cameras are used on opposite sides of the sample. The strain tensors components ($\varepsilon_{\theta\theta}$, ε_{zz}, $\varepsilon_{\theta z}$) and the displacement gaps (vertical Δu_z and rotation Δu_θ) are calculated on each side. Then, for each quantity, the two obtained values are averaged. The average values are used for the mechanical analysis of the sample.

3 Interface mechanical properties

3.1 Asphalt complex moduli and complex interface stiffnesses definitions

The axial stress σ_{zz} and the shear stress $\tau_{\theta z}$ in the sample are obtained from load cells measurement considering equations (1) and (2). These equations are derived with the assumption that stress field is homogeneous in the sample:

$$\sigma_{zz} = \frac{F}{A} \tag{1}$$

where *F* is the axial force measured with press load cell and *A* the section area of the hollow cylinder, and:

$$\tau_{\theta z} = \frac{3T}{2\pi * (R_{ext}^3 - R_{int}^3)} \tag{2}$$

where *T* is the torque measured with press load cell, R_{ext} the external radius and R_{int} the internal radius.

For a small number of applied loading cycles and for small loadings amplitudes, conditions similar to those existing in a real pavement, asphalt concretes present a linear viscoelastic (LVE) behavior [39]. For a sinusoidal loading in stress control mode, the LVE material strain response is also a sinusoidal signal with a phase lag.

For an axial stress sinusoidal signal σ_{zz} such as equation (3), the strain tensor component ε_{zz} is given in equation (4).

$$\sigma_{zz}\,(t) = \sigma_{zz\_0}\ sin(\omega t) \tag{3}$$

$$\varepsilon_{zz}\,(t) = \varepsilon_{zz\_0}\ sin(\omega t - \varphi_E) \tag{4}$$

where σ_{zz_0} is the vertical stress amplitude, ε_{zz_0} the vertical strain amplitude and φ_E the phase angle.

The Young's complex modulus E_{zz}* is defined in equation (5):

$$E_{zz}^* = \frac{\sigma_{zz\_0}}{\varepsilon_{zz\_0}}\ e^{i\varphi_E} = |E_{zz}^*|e^{i\varphi_E} \tag{5}$$

When shear stress is applied, for example $\tau_{\theta z}$ in direction "θz", the complex shear modulus $G_{\theta z}$* is given in equation (6):

$$G_{\theta z}^* = \frac{\tau_{\theta z\_0}}{2\varepsilon_{\theta z\_0}}\ e^{i\varphi_G} = |G_{\theta z}^*|e^{i\varphi_G} \tag{6}$$

with $\tau_{\theta z\_0}$ the amplitude of shear stress and $\varepsilon_{\theta z\_0}$ the shear strain amplitude. φ_G is the phase angle in shear mode.

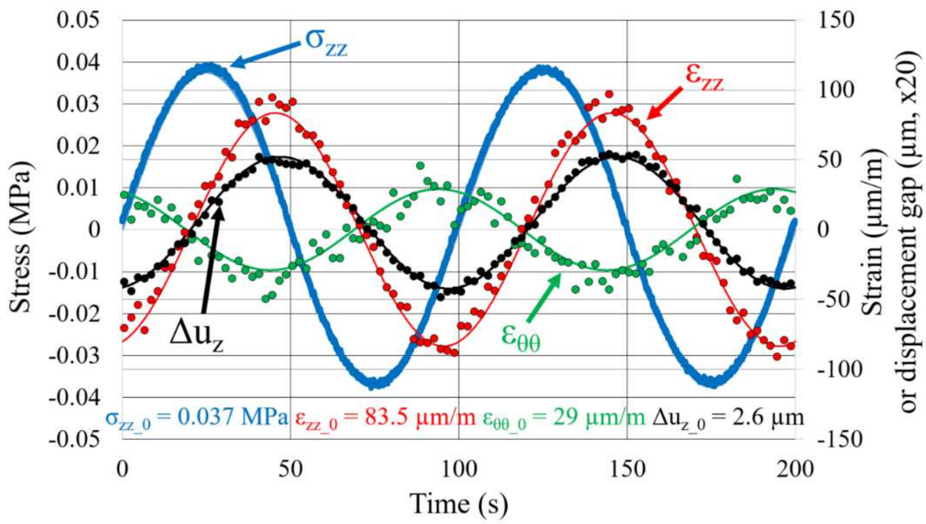

Fig. 9. Example of stress, strain and displacement gap measurements in one layer and at the interface for an axial test (with least square approximations in continuous lines)

It is observed that when a sinusoidal stress signal is applied to the interface, displacement gaps are also sinusoidal (as in Figure 9). It is then possible to define a complex interface stiffness.

The normal complex interface stiffness K_{zz}* is defined in equation (7).

$$K^*_{zz} = \frac{\sigma_{zz\_0}}{\Delta u_{z\_0}} \; e^{i\varphi_{Kzz}} = |K^*_{zz}| e^{i\varphi_{Kzz}} \tag{7}$$

with Δu_{z_0} the amplitude of the vertical displacement gap at the interface. φ_{Kzz} is the phase angle for interfaces in tension-compression mode.

If torsion is applied, the shear complex interface stiffness $K_{\theta z}$* is given in equation (8).

$$K^*_{\theta z} = \frac{\tau_{\theta z\_0}}{\Delta u_{\theta\_0}} \; e^{i\varphi_{K\theta z}} = |K^*_{\theta z}| e^{i\varphi_{K\theta z}} \tag{8}$$

with Δu_{θ_0} the amplitude of the horizontal (tangential) displacement gap at the interface. $\varphi_{K\theta z}$ is the phase angle for interfaces in shear mode.

The complex Poisson's ratio $\nu_{\theta z}$* in each layer can also be found using equation (9):

$$\nu^*_{\theta z} = \frac{\varepsilon_{\theta\theta\_0}}{\varepsilon_{zz\_0}} \; e^{i\varphi_{\nu\theta z}} = |\nu^*_{\theta z}| e^{i\varphi_{\nu\theta z}} \tag{9}$$

with $\varepsilon_{\theta\theta\_0}$ the amplitude of the relative variation of cylinder perimeter. $\varphi_{\nu\theta z}$ is the phase angle for Poisson's ratio.

3.2 Procedure and tested material

One sample with two asphalt concrete layers and a tack coat at the interface has been tested. The upper layer was in BBSG3 0/10 [40], representing the wearing course of a pavement, and the lower layer was in GB5® 0/14, usually used as a base course. The two layers had the same thickness. The tack coat is a bituminous emulsion of pure bitumen with a residual dosage of 350 g/m^2.

In order to characterize the viscoelastic properties of the interface and of the asphalt concretes, sinusoidal loading cycles at small strain amplitude were applied to the sample. The tests presented in this paper were performed at four different temperatures (about 10, 20, 30, and 40 °C). At each temperature, two types of tests were done successively: axial tests and rotation tests (Table 1). During axial tests, vertical displacement was controlled with the averaged value of the two vertical non-contact sensors while torque was maintained nil. During rotation tests, rotation displacement was controlled with the averaged value of the horizontal non-contact sensors and axial force was maintained at a very small compressive value (around 15 kPa). The amplitude values for non-contact sensors were calculated in order to get 200 µm/m in global vertical strain ε_{zz} (corresponding to the case where the sample would be constituted of one homogeneous material) for axial tests and 200 µm/m in global shear strain $\varepsilon_{\theta z}$ for rotation tests. For each type of test, four frequencies were tested with five sinusoidal cycles applied for each frequency.

Table 1. Mechanical loading for each temperature

Type of test	**Axial loading**	**Torsion loading**	**Frequencies (Hz)**	**Amplitude Non-contact sensors**	**Cycles per frequency**
Axial	Sinusoidal displacement	Zero torque	0.01; 0.03; 0.1; 0.3	ax = 25 µm	5
Rotation	Small compression 15 kPa	Sinusoidal displacement		rot = 90 µm	5

Each camera took 50 pictures of the sample per cycle (Figure 10) except for cycles at 0.3 Hz where 30 pictures were taken at each cycle. The subset size for DIC was 21 x 21 pixels, which corresponds to 3.1 x 3.1 mm^2 on the material. The capture time of a picture was 6 ms.

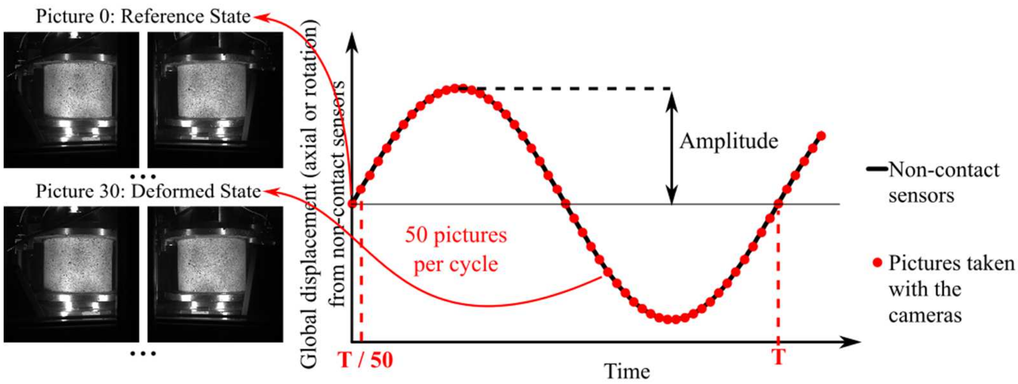

Fig. 10. Global displacement from non-contact sensors and acquisition of pictures on one side of the sample during the tests (T is the loading period)

3.3 Results and discussion

All stress and strain signals were fitted with sinusoidal functions using the least square method before being analyzed. An indicator was used to quantify and check the signal quality. With 3D DIC, the measured vertical strain amplitudes ε_{zz_0} for axial tests ranged from 200 to 250 µm/m in the upper layer and from 100 to 150 µm/m in the lower layer, the vertical displacement gap amplitude Δu_{z_0} being between 1 and 3.5 µm. $\varepsilon_{\theta\theta}$ amplitude was between 70 and 100 µm/m in the upper layer and between 25 and 50 µm/m in the lower layer. For rotation tests, the shear strain amplitudes $\varepsilon_{\theta z\_0}$ were between 250 and 350 µm/m in the upper layer and between 75 and 100 µm/m in the lower layer, the rotation displacement gap amplitude Δu_{θ_0} was between 4 and 8 µm/m. The difference in strain values between the two layers is related to the difference in modulus between the two asphalt concretes, it depends on the temperature and the frequency.

For the asphalt concretes layers, isothermal curves of the Young's complex modulus norm $|E_{zz}^*|$ are shown in the Figure 11 and isothermal curves of the complex shear modulus norm $|G_{\theta z}^*|$ are represented in Figure 12.

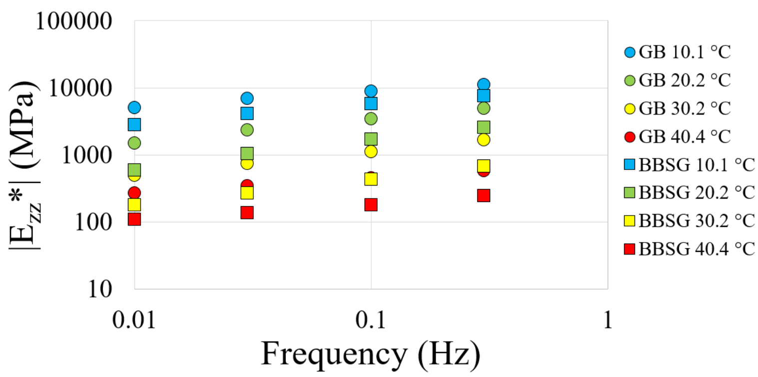

Fig. 11. Isothermal curves of Young's complex modulus norm $|E_{zz}*|$ for asphalt concretes in the upper layer (BBSG) and in the lower layer (GB)

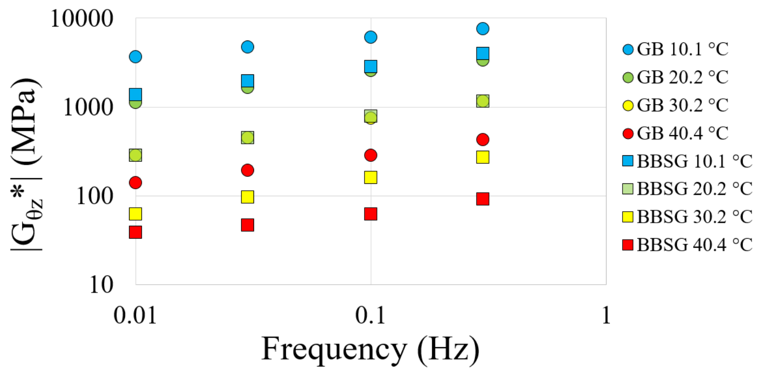

Fig. 12. Isothermal curves of complex shear modulus $|G_{\theta z}*|$ for asphalt concretes in the upper layer (BBSG) and in the lower layer (GB)

The BBSG 3 asphalt concrete is less rigid than the GB5® at the same temperature and frequency. This can be seen in axial tests (Figure 11) and in rotation tests (Figure 12) and is consistent with the specifications of these asphalt concretes.

Isotherms of normal complex interface stiffness norm $|K_{zz}*|$ obtained from axial tests and shear complex interface stiffness norm $|K_{\theta z}*|$ obtained from the rotation tests are presented in Figure 13. Interfaces are more rigid in tension-compression mode than in shear mode.

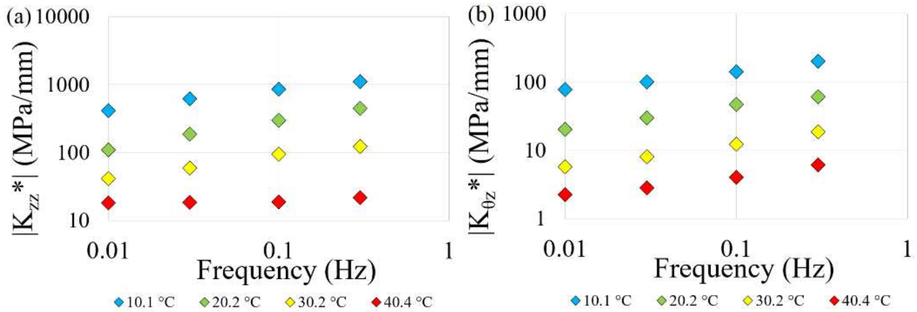

Fig. 13. (a) Isothermal curves of normal complex interface stiffness norm $|K_{zz}*|$ for axial tests and (b) isothermal curves of shear complex interface stiffness norm $|K_{\theta z}*|$ for rotation tests

The isotherms of complex Poisson's ratio norm $|\nu_{\theta z}*|$ in the upper (BBSG) layer and in the lower (GB) layer are presented in Figure 14 for axial tests. Poisson's ratios values are between 0.3 and 0.4 which is a good order of magnitude for asphalt concretes at these temperatures and frequencies [41]. No significant differences could be observed between the two layers.

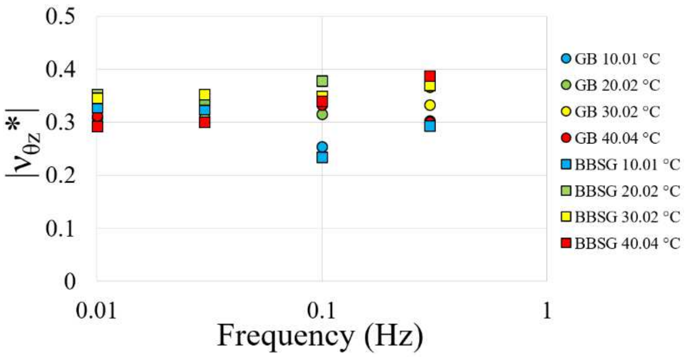

Fig. 14. Isothermal curves of complex Poisson's ratio norm $|\nu_{\theta z}^*|$ for asphalt concretes in the upper layer (BBSG) and in the lower layer (GB)

4 Conclusions

The 2T3C Hollow Cylinder Apparatus (2T3C HCA) is an innovative prototype with unique characteristics to study the interfaces between pavement layers. It can apply torsion and/or tension-compression independently to hollow cylinder samples. The tests can be cyclic or monotonic with temperature control. The thickness of the wall is small regarding the external diameter so the stress distribution can be considered as homogeneous in the sample.

3D DIC measurements and the developed analysis method enable to obtain the strain tensor components ($\varepsilon_{\theta\theta}$, ε_{zz}, $\varepsilon_{\theta z}$) of both asphalt concrete layers and the displacement gaps at the interface (vertical Δu_z and rotation Δu_θ). The Young's and shear complex moduli (E_{zz}^*, $G_{\theta z}^*$) and Poisson's ratio ($\nu_{\theta z}^*$) of the two asphalt mixes and the complex interface stiffnesses (K_{zz}^*, $K_{\theta z}^*$) are obtained.

In this paper, tests at four temperatures (from 10 °C to 40 °C) and four frequencies (from 0.01 Hz to 0.3 Hz) in shear mode and in tension-compression mode were performed on a sample with two asphalt layers and a tack coat at the interface. The following conclusions were drawn from these tests:

1) Presented results show the accuracy and efficiency of the 2T3C HCA prototype to study interfaces in the small strain domain.

2) Displacement gaps with amplitudes as low as 1 µm were observed. Magnitude of measured strain amplitude in asphalt layers was of some 10^{-5} m/m.

3) The interfaces seem more rigid in tension-compression than in shear.

The developed 2T3C HCA device appears as a powerful experimental tool to investigate interface properties between bituminous layers.

References

1. Uzan, J., Livneh, H. & Eshed, Y. Investigation of adhesion properties between asphaltic-concrete layers. in **47,** 495–521 (1978).

2. Diakhaté, M. Fatigue et comportement des couches d'accrochage dans les structures de chaussée. (2007).

3. LCPC & SETRA. *Conception et dimensionnement des structures de chaussée*. (1994).

4. AASHTO. *Guide for design of Pavement Structure*. (2002).

5. Meunier, Y. Le décollement des couches de revêtement de chaussées. (1986).

6. Blomberg, J. Tack Coat Specifications and Testing. Presented at the North Central Asphalt User Producer Group Technical Conference (2014).

7. Petit, C., Diakhaté, M., Millien, A., Phelipot-Mardelé, A. & Pouteau, B. Pavement design for curved road sections: fatigue performance of interfaces and longitudinal top-down cracking in multilayered pavements. *Road Mater. Pavement Des.* **10,** 609–624 (2009).

8. Leutner, R. Untersuchung des Schichtenverbundes beim bituminosen Oberbau. **41,** 84–91 (1979).

9. Tschegg, E. K., Kroyer, G., Tan, D.-M., Stanzl-Tschegg, S. E. & Litzka, J. Investigation of Bonding between Asphalt Layers on Road Construction. *J. Transp. Eng.* **121,** 309–316 (1995).

10. Canestrari, F., Ferrotti, G., Partl, M. & Santagata, E. Advanced Testing and Characterization of Interlayer Shear Resistance. *Transp. Res. Rec. J. Transp. Res. Board* **1929,** 69–78 (2005).

11. Zofka, A. *et al.* Advanced shear tester for evaluation of asphalt concrete under constant normal stiffness conditions. *Road Mater. Pavement Des.* **16,** 187–210 (2015).

12. Zhao, H., Cao, J. & Zheng, Y. Investigation of the interface bonding between concrete slab and asphalt overlay. *Road Mater. Pavement Des.* **18,** 109–118 (2017).

13. Brühwiler, E. & Wittmann, F. H. The wedge splitting test, a new method of performing stable fracture mechanics tests. *Eng. Fract. Mech.* **35,** 117–125 (1990).

14. Collop, A. C., Sutanto, M. H., Airey, G. D. & Elliott, R. C. Development of an automatic torque test to measure the shear bond strength between asphalt. *Constr. Build. Mater.* **25,** 623–629 (2011).

15. Canestrari, F. *et al.* Mechanical Testing of Interlayer Bonding in Asphalt Pavements. in *Advances in Interlaboratory Testing and Evaluation of Bituminous Materials* (eds. Partl, M. N. et al.) **9,** 303–360 (Springer Netherlands, 2013).

16. Raposeiras, A. C., Castro-Fresno, D., Vega-Zamanillo, A. & Rodriguez-Hernandez, J. Test methods and influential factors for analysis of bonding between bituminous pavement layers. *Constr. Build. Mater.* **43,** 372–381 (2013).

17. Graziani, A., Canestrari, F., Cardone, F. & Ferrotti, G. Time–temperature superposition principle for interlayer shear strength of bituminous pavements. *Road Mater. Pavement Des.* **18,** 12–25 (2017).

18. Mohammad, L., Raqib, M. & Huang, B. Influence of asphalt tack coat materials on interface shear strength. *Transp. Res. Rec. J. Transp. Res. Board* 56–65 (2002).

19. Tozzo, C., D'Andrea, A., Cozzani, D. & Meo, A. Fatigue Investigation of the Interface Shear Performance in Asphalt Pavement. *Mod. Appl. Sci.* **8,** (2014).

20. D'Andrea, A. & Tozzo, C. Dynamic tests on bituminous layers interface. *Mater. Struct.* **49,** 917–928 (2016).

21. Isailović, I., Wistuba, M., Büchler, S. & Falchetto, A. Interface shear fatigue performance of asphalt pavement structures in function of normal stress and temperature. in 1525–1530 (2017). doi:10.1201/9781315100333-218

22. Raab, C., Partl, M., Fourquet, E. & AbdElHalim, A. Static and cyclic evaluation of interlayer bonding. in *Bearing Capacity of Roads, Railways and Airfields* 1511–1516 (2017). doi:10.1201/9781315100333-216

23. Sayao A. & Vaid, Y. P. A critical assessment of stress nonuniformities in hollow cylinder test specimens. *Soils Found.* **31,** 60–72 (1991).

24. Hight, D. W., Gens, A. & Symes, M. J. The development of a new hollow cylinder apparatus for investigating the effects of principal stress rotation in soils. *Géotechnique* **33,** 355–383 (1983).

25. Duttine, A., Di Benedetto, H., Bang, D. P. V. & Ezaoui, A. Anisotropic small strain elastic properties of sands and mixture of sand-clay measured by dynamic and static methods. *Soils Found.* **47,** 457–472 (2007).

26. Sousa, J. B. Dynamic properties of materials for pavement design. (University of California, Berkeley, 1986).

27. Brown, S. F., Brodrick, B. V., Tekieli, K. & Collop, A. C. A torsional hollow cylinder research apparatus for studying the permanent deformation characteristics of asphalt. *Road Mater. Pavement Des.* **14,** 65–85 (2013).

28. Rueda, E. J., Caro, S., Caicedo, B. & Monroy, J. A new approach for the advanced mechanical characterisation of asphalt mixtures using the hollow cylinder methodology. *Measurement* **103**, 333–342 (2017).

29. NF EN 12697-33+A1 Septembre 2007 Mélange bitumineux - Méthodes d'essai pour mélange hydrocarboné à chaud - Partie 33 : confection d'éprouvettes au compacteur de plaque.

30. Sutton, M. A., Wolters, W. J., Peters, W. H., Ranson, W. F. & McNeill, S. R. Determination of displacements using an improved digital correlation method. *Image Vis. Comput.* **1,** 133–139 (1983).

31. Romeo, E. Two-dimensional digital image correlation for asphalt mixture characterisation: interest and limitations. *Road Mater. Pavement Des.* **14,** 747–763 (2013).

32. Buttlar, W. G. *et al.* Digital image correlation techniques to investigate strain fields and cracking phenomena in asphalt materials. *Mater. Struct.* **47,** 1373–1390 (2014).

33. Ktari, R., Millien, A., Fouchal, F., Pop, I.-O. & Petit, C. Pavement interface damage behavior in tension monotonic loading. *Constr. Build. Mater.* **106,** 430–442 (2016).

34. Golewski, G. L. Estimation of the optimum content of fly ash in concrete composite based on the analysis of fracture toughness tests using various measuring systems. *Constr. Build. Mater.* **213***,* 142–155 (2019).

35. Golewski, G. L. Measurement of fracture mechanics parameters of concrete containing fly ash thanks to use of Digital Image Correlation (DIC) method. *Measurement*. **135**, 96–105 (2019).

36. Jin, T., Ha, N. S., Le, V. T., Goo, N. S. & Jeon, H. C. Thermal buckling measurement of a laminated composite plate under a uniform temperature distribution using the digital image correlation method. *Compos. Struct.***123**, 420–429 (2015).

37. Chemisky, Y., Meraghni, F., Bourgeois, N., Cornell, S., Echchorfi, R. & Patoor, E. Analysis of the deformation paths and thermomechanical parameter identification of a shape memory alloy using digital image correlation over heterogeneous tests. *Int. J. Mech. Sci.***96-97**, 13–24 (2015).

38. Sutton, M. A., McNeill, S. R., Helm, J. D. & Chao, Y. J. Advances in two-dimensional and three-dimensional computer vision. in *Photomechanics* 323–372 (2000).

39. Gayte, P., Di Benedetto, H., Sauzéat, C. & Nguyen, Q. T. Influence of transient effects for analysis of complex modulus tests on bituminous mixtures. *Road Mater. Pavement Des.* **17**, 271–289 (2016).

40. NF EN 13108-1 Septembre 2007 Mélange bitumineux - Spécification des matériaux - Partie 1 : Enrobés bitumineux.

41. Perraton, D. *et al.* 3Dim experimental investigation of linear viscoelastic properties of bituminous mixtures. *Mater. Struct.* **49,** 4813–4829 (2016).